Is the relation between the solar wind dynamic pressure and the magnetopause standoff distance so straightforward?

A. A. Samsonov[1], Y. V. Bogdanova[2], G. Branduardi-Raymont[1], D. G. Sibeck[3], G. Tóth[4]

[1]Mullard Space Science Laboratory, University College London, UK
[2]RAL Space,Rutherford Appleton Laboratory, Science and Technology Facilities Council, UK
[3]NASA, Goddard Space Flight Center, Greenbelt, MD, USA
[4]Department of Climate and Space, University of Michigan, Ann Arbor, Michigan, USA

Key Points:

- We reconsider the relation between the solar wind dynamic pressure and magnetopause standoff distance
- The magnetopause reacts differently to density and velocity increases for the same dynamic pressure
- A new scaling law for magnetopause standoff distance is proposed

Corresponding author: Andrey Samsonov, a.samsonov@ucl.ac.uk

Abstract

We present results of global magnetohydrodynamic simulations which reconsider the relationship between the solar wind dynamic pressure (P_d) and magnetopause stand-off distance (R_{SUB}). We simulate the magnetospheric response to increases in the dynamic pressure by varying separately the solar wind density or velocity for northward and southward interplanetary magnetic field (IMF). We obtain different values of the power laws indices N in the relation $R_{SUB} \sim P_d^{-1/N}$ depending on which parameter, density or velocity, has been varied and for which IMF orientation. The changes in the stand-off distance are smaller (higher N) for a density increase for southward IMF and greater (smaller N) for a velocity increase. An enhancement of the solar wind velocity for a southward IMF increases the magnetopause reconnection rate and Region 1 current that move the magnetopause closer to the Earth than it appears in the case of density increase for the same dynamic pressure.

Plain Language Summary

The magnetopause is the boundary between the near-Earth space, which is governed by the magnetic field produced in the Earth's core, and interplanetary space populated by the plasma emitted from the Sun called the solar wind. It is well-known that the position of this boundary is defined by the balance of the pressures from both sides of the magnetopause and in a unique way depends on the velocity and density of the plasma in the interplanetary space. In this work, we re-examine the relationship between the magnetopause position and parameters of the solar wind by means of computer modelling. It is shown that the relationship between solar wind velocity and density and magnetopause position is more complex than originally thought. It is suggested that the pressure balance condition through the magnetopause depends on the continuing magnetic reconnection between the interplanetary and magnetospheric magnetic field lines, and that the consequences of the reconnection change the relationship between the solar wind dynamic pressure and magnetopause boundary location.

1 Introduction

The magnetopause is one of principal magnetospheric boundaries which separates dense solar wind plasma in the magnetosheath and tenuous and hot magnetospheric plasma. In response to strong solar wind pressure pulses, the magnetopause comes closer to the Earth and geosynchronous spacecraft may exit the magnetosphere and cross the magnetosheath in the subsolar region or even enter into the supersonic solar wind. To date, more than 15 empirical models of the magnetopause have been developed based on a great number of magnetopause crossings under different solar wind conditions (a list of 14 models published by (Suvorova & Dmitriev, 2015)). Chapman and Ferraro (1931) suggested that the magnetopause location can be determined from the pressure balance condition between the solar wind dynamic pressure (P_d) and the magnetic pressure of the Earth's dipole. Besides the dynamic pressure, the second important solar wind parameter influencing the magnetopause position is the interplanetary magnetic field (IMF) B_z component (Aubry et al., 1970; Fairfield, 1971). A strong southward IMF ($B_z < 0$) results in magnetic reconnection at the dayside magnetopause and intensification of the large scale field-aligned (Region 1) currents connecting the magnetosphere and ionosphere and moving the magnetopause closer to the Earth (Hill & Rassbach, 1975; Sibeck, 1994). The P_d and B_z are the only two input parameters in several popular magnetopause models, e.g. (Petrinec & Russell, 1996; Roelof & Sibeck, 1993; Shue et al., 1997; Shue et al., 1998; Sibeck et al., 1991). The recent (Lin et al., 2010) empirical model replaces the solar wind dynamic pressure by the sum of dynamic and magnetic pressures and takes into account the Earth's dipole tilt. Moreover, several papers (Dušík et al., 2010; Grygorov et al., 2017; Merka et al., 2003; Samsonov et al., 2017; Suvorova et al., 2010) note that the magne-

topause significantly expands during radial IMF intervals concluding that the IMF cone angle (the angle between IMF and the Sun-Earth line) may also be an important parameter for calculation of the magnetopause location.

Recently, Němeček et al. (2016) compared observed magnetopause crossings with the Shue et al. model (Shue et al., 1997) for half of the last solar cycle and found systematic differences between the model and observations. They argued that the ionospheric conductivity and the solar wind velocity are additional parameters that influence the magnetopause position. Their statistical analysis shows that the average magnetopause is farther from the Earth than predicted during time intervals with lower conductivity and higher solar wind velocity. They suggested that intensification of UV radiation results in an increase in the magnetospheric-ionospheric currents that decreases the magnetic pressure inside the magnetosphere and the magnetopause moves earthward. On the contrary, enhancement of the velocity intensifies the viscous interaction between the solar wind and magnetosphere increasing the global magnetospheric convection and bringing more magnetic flux to the dayside magnetosphere. We will discuss these assumptions below in the paper.

Another topic under debate is the power law index in the relation between the P_d and the magnetopause standoff distance R_{SUB}. The simple pressure balance condition predicts

$$R_{SUB} \sim P_d^{-1/N} \tag{1}$$

with $N = 6$ (Beard, 1960), however most empirical models use other power law indices, both larger and smaller than the theoretical one, e.g. $N = 6.6$ in (Shue et al., 1998) and $N = 5.263$ (for the sum of dynamic and magnetic pressures) in (Lin et al., 2010). Dušík et al. (2010) studied variations of the observed magnetopause location in dependence on the dynamic pressure and IMF cone angle and obtained $N = 4.8$. Lu et al. (2011) used MHD simulations to derive the relation between solar wind parameters and magnetopause position and obtained $N = 5.2$. Liu et al. (2015) continued to develop this approach taking into account more input parameters than in Lu et al. (2011) and found $N = 5.89$. We note, however, the limitation of the above studies in calculations of the R_{SUB}. Empirical models use magnetopause crossings over a large area and have to assume some functional dependence for the magnetopause shape. Even in the MHD simulations, Lu et al. (2011) and Liu et al. (2015) used a modified function developed from one suggested by Shue et al. (1997) and applied multiple parameter fitting to find unknown coefficients.

In this study, we focus our attention on variations of the magnetopause standoff distance and use several versions of recent global MHD models to study the dependence of the R_{SUB} on solar wind parameters. In particular, we reconsider the relation between R_{SUB} and P_d. Since dynamic pressure is a product of the density and velocity square, both density and velocity variations make input in the P_d changes. However, MHD models allow us to get magnetospheric response to artificial solar wind variations and investigate how the standoff distance depends on the density and velocity independently of each other.

2 MHD simulations

We use the Space Weather Modeling Framework (SWMF) global MHD model (Tóth et al., 2005, 2012) coupled and also noncoupled with the Comprehensive Inner-Magnetosphere Ionosphere (CIMI) Model (Fok et al., 2014) and the Lyon-Fedder-Mobarry magnetosphere–ionosphere model (LFM–MIX) (Lyon et al., 2004; Merkin & Lyon, 2010). The models are available through Community Coordinated Modeling Center (CCMC) runs on request. We employ several versions of the SWMF model (as explained below) and only one version of the LFM model for comparison. The grid spacing near the dayside magnetopause is 0.25 R_E for the SWMF model; the grid spacing for the LFM-MIX model

is of the same order of magnitude but non-uniform depending on the geocentric distance and direction. The magnetopause position is determined as the boundary between open and closed field lines and calculated by CCMC software for every run.

For each version of the models, we make four runs. In run 1, we increase only the solar wind density and keep constant all other parameters. In run 2, we increase the solar wind velocity in a such way to get exactly the same variations of the dynamic pressure as in run 1. All other parameters are the same and the IMF is northward in these two runs. In runs 3 and 4, we impose the same variations of the density and velocity as in runs 1 and 2 respectively but for a southward IMF, the IMF magnitude being the same in all runs. The variations of the solar wind dynamic pressure (the same in all runs) are shown in Figure 1. The P_d grows from 0.8 to 8.0 nPa, this corresponds to an increase in density from 3 to 30 cm^{-3} or to an increase in velocity from 309.84 to 979.80 km/s for the fixed other parameter. In those runs when we keep these parameters constant, the density is 5 cm^{-3} and the velocity is 400 km/s which is close to the averages. The IMF components are equal to (-2,2,$\pm$4) nT.

Figure 2 shows the changes in the magnetopause standoff distance with time in the four runs for the noncoupled SWMF model (v20140611). The left panel corresponds to runs 1-2, and the right panel corresponds to runs 3-4; blue and red lines indicate results for the density and velocity increases respectively. For comparison, we also show results of the (Shue et al., 1998) and (Lin et al., 2010) empirical models which depend on the dynamic pressure and B_z, but give the same response for the density and velocity changes (i.e. if comparing runs 1 and 2, or 3 and 4). However, the MHD model does not predict the same variations in the magnetopause standoff distance for the density and velocity increases. It becomes very clear, in particular for the southward IMF, that the slope of the red line is greater than of the blue line, i.e. the change in R_{SUB} is higher for the velocity increase. The northward case displays a difference in the density and velocity runs too, but the effect is weaker than in the southward case. In general, the slope of the MHD curves is similar to that in the (Shue et al., 1998) model, but less than in the (Lin et al., 2010) model.

When pressure pulses arrive at the subsolar point, the magnetopause is briefly overcompressed and then relaxes to a new equilibrium. The overcompression is probably related to fast compressional waves in the magnetosphere moving earthward at the beginning of compression and being reflected from the inner boundary in the numerical models (Samsonov et al., 2007; Samsonov & Sibeck, 2013), and from the ionosphere or plasmapause in the observations (Samsonov et al., 2011). When the reflected wave reaches the magnetopause, the inward magnetopause motion is replaced by outward motion. Several cycles of heavy damped magnetic field oscillations may be excited in the dayside magnetosphere (Freeman et al., 1995; Němeček et al., 2011; Samsonov et al., 2011). However, we ignore these temporal variations in the present work and exploit only final quasi-stationary positions. Note that the time interval between two step-like increases in the density or velocity is 20 min, which is shown to be enough to establish a new equilibrium. We have considered a time interval twice as long (i.e. 40 min instead of 20 min) in another run and obtained very similar results.

Next, we show the dependence between the R_{SUB} and P_d in logarithmic scale in Figure 3. Equilibrium points in the MHD simulations are shown by red crosses. Blue lines display linear interpolation of the MHD points. In all runs, the simulation points are well interpolated by straight lines with the corrected standard deviations of about 0.001. The coefficients of the linear interpolation provide the power law index in (1), and we collect these numbers in Table 1 below.

We suggest that the difference in the magnetospheric response to the density and velocity increases is explained by magnetopause magnetic reconnection. If the density increases and the velocity is constant, even for a southward IMF, the solar wind elec-

tric field remains the same and the magnetopause reconnection rate would vary insignificantly. On the contrary, if the velocity increases, the electric field and reconnection rate increase too. In turn, this enhances the magnetospheric-ionospheric currents, in particular the Region 1 current. The intensification of this current system weakens the magnetospheric magnetic field and moves the dayside magnetopause earthward, in the same way as occurs in the case of southward IMF turning (Sibeck, 1994).

We show the y component of the magnetosheath electric field in the inflow region (at the sunward boundary of the magnetopause current layer), absolute reconnection rate, the ratio of the inflow velocity to the magnetosheath Alfven speed, and the reconnection rate normalized to the total solar wind electric field in Figure S2 in Supporting information. The reconnection rate has been calculated at the boundaries of the magnetopause current layer as explained in Cassak and Shay (2007), Borovsky et al. (2008), Borovsky and Birn (2014). (Figure S1 and the corresponding explanation in Supporting information provide additional information on the method.) We find that the difference in the magnetosheath electric field and reconnection rate between the two runs with density and velocity increases is related to the difference in the solar wind electric field, and for the case with the increased velocity the absolute reconnection rate (as well as the Ey electric field) in the inflow region increases with time and at the end of simulation run becomes 2.5 times larger than the absolute reconnection rate (or Ey) for the case with the increased density. However, the reconnection rates normalized to the solar wind electric field are nearly the same in both runs and slightly decrease during the runs from about 0.55 to 0.4. These values are close to those obtained in simulation A in Borovsky et al. (2008).

Higher reconnection rate intensifies the Region 1 current and increases the cross polar cap potential (CPCP). Figure S3 shows temporal variations of the CPCP in four runs. For the both northward and southward IMF, the CPCP grows faster in the case of velocity increase, but again the difference becomes substantial for the southward IMF. The CPCP seems to remain mainly below a saturation level (Hill et al., 1976; Siscoe et al., 2002), although it might be close to the saturation for a largest CPCP used in this work (southward IMF, high velocity). Anyway, we do not observe the effect of saturation on the magnetopause location, e.g. while considering the dependencies in Figure 3.

The increases in the CPCP in Figure S3 are accompanied by overshoots and undershoots, especially in runs 2 and 4 with the velocity increase. The reason of these transients could be explained by the following. Both the density and velocity jumps are nonstationary structures because both of them do not meet the Rankine–Hugoniot relations. In the both cases, the total pressure increases through the discontinuities but the increase in the velocity immediately results in an increase in the density while the structure propagating in the solar wind from the inflow boundary to the bow shock. This may cause a larger increase in the dynamic pressure near the magnetopause. We have inspected a possible increase in the density near the subsolar bow shock in runs 2 and 4 and found that the solar wind density really increases at the jumps in velocity, but only at several first jumps. If the solar wind velocity is low, the propagation time from the inflow boundary to the bow shock is long so the density has enough time to pile up. However, the density enhancement drops below 1% for the velocity higher than 500 km/s. Since this effect is negligible most of the time, we think that it does not influence the slopes in Figure 3. Besides, the increases in the solar wind velocity results in other discontinuities in the magnetosheath and magnetosphere as those forward and reflected compressional waves mentioned above. Anyway, we use only quasi steady-state values after the transients in our study.

Another signature of the enhanced magnetic reconnection can be observed at dayside geosynchronous orbit. Figure S4 compares variations of the magnetic field magnitude for the same runs on the Sun-Earth line at $x = 6.6$ R_E. Since magnetopause reconnection is stronger for high velocity (electric field) and southward IMF (run 4), we

eventually get a weaker magnetic field at geosynchronous orbit in this case. The difference in the magnetic field magnitude between runs 1 (density increase for northward IMF) and 4 (velocity increase for southward IMF) grows with the solar wind dynamic pressure from 7 (t=03:00) to 16 (t=07:00) nT.

Using relatively short (20 min) time intervals between the dynamic pressure steps, we implicitly assume that the changes in the magnetopause position mostly result from the changes in the solar wind pressure and variations of the dayside field-aligned Region 1 currents. Meanwhile, Tsyganenko and Sibeck (1994) noted that the cross-tail current and in a less degree the ring current besides the Region 1 currents determine the magnetic field on the magnetospheric side of the magnetopause. An increase in the magnetotail current as well increase in the Region 1 currents weakens the magnetospheric magnetic field and moves the dayside magnetopause earthward. Although the magnetotail current may have a slightly larger response time, but in general it only intensifies the effect of the Region 1 current. On the contrary, an enhanced ring current during magnetic storms may push the subsolar magnetopause outward (e.g., some estimations were made in Samsonov et al. (2016)), however (1) the noncoupled MHD model which results have been presented above does not reproduce the ring current and (2) the time scale of the ring current intensification is usually more than the 3-4 hours used in these simulations. We show results of the coupled models below which qualitatively similar to the results of the noncoupled model, so this does not change our conclusions.

Finally, we would like to compare several runs to confirm that our results are model-independent. Table 1 collects the power law indices N in (1) calculated from six versions of three global MHD models. The first is the non-coupled SWMF model whose results were presented above. In addition to the basic runs (version 1), we simulated three other versions of the the same non-coupled model, two with a higher ionospheric conductivity and one with a dipole tilt. The height-integrated Pedersen conductivity is assumed to be equal to 5 S in all the versions, except versions 2 and 3 for which the integrated conductivity is 10 and 100 S respectively. In version 4, we simulated the magnetosphere with a dipole tilt 30°. Changes in N between versions 1 and 2 and versions 1 and 4 are small, and between versions 1 and 3 are moderate, but only for the southward IMF. Note that the ionospheric conductivity 100 S is extremely high and can be hardly observed in reality. We show it only to illustrate the role of conductivity since the two times increase in conductivity in version 2 changes N only for the velocity increase with southward IMF.

Version 5 stands for runs of the SWMF model coupled with CIMI (inner magnetosphere-ionosphere), and version 6 is the LFM-MIX model. For each version, we make four runs for the northward/southward IMF and for the density and velocity increases as explained above (24 runs in total). Recall that $N = 6$ in the ideal theoretical case if the magnetopause position meets the pressure balance between the solar wind dynamic pressure and the Earth's dipole field and $N = 6.6$ in the empirical (Shue et al., 1998) model. In fact, most of the obtained N are between these two values or slightly less. Five of six versions predict N larger or equal to 7 in the runs with the density increase for southward IMF. Even if version 5 predicts N smaller than 7, N is systematically highest in this case for every model.

In addition to the comparison of different models, we investigate the influence of grid resolution on our results. We have calculated two runs for the same southward IMF with density and velocity changes using the non-coupled SWMF model with the 1/16 R_E grid spacing around the subsolar magnetopause. We obtain different power laws, N=6.712 and 6.132, in the density and velocity runs respectively (instead of 7.80 and 6.69 for the same model with a low resolution). Moreover, the normalized (to the solar wind electric field) reconnection rates in the low resolution runs are smaller than those in the high resolution runs (but are about the same in the density and velocity runs for the same resolution). We also find some differences in the CPCP and the magnetic field magni-

tude at geosynchronous orbit. We note that the grid resolution influences the magnitude of maximal electric current density at the magnetopause and possibly may change the total magnetopause current, but this problem requires more careful studies and it stays outside of the scope of the paper.

Even if the models predict different N, the relations between the runs 1-4 in Table 1 are similar for all models. (1) For all models except one case, the runs with velocity increase correspond to a smaller N than the runs with density increase, however the difference between the density and velocity runs is substantial only for the southward IMF. On the contrary, N is slightly higher in the velocity run than in the density run for the case with northward IMF and tilted dipole. (2) In the runs with density increase, N is always smaller for the northward IMF than for the southward IMF. (3) In the cases with two times higher ionospheric conductivity (10 S instead of 5 S) or with 30° dipole tilt, N changes relatively small. However, a significant increase in the ionospheric conductivity up to 100 S (what is probably unrealistic) or inclusion of the inner magnetosphere - ionosphere block in the model results in decrease in N. To be precise, the high ionospheric conductivity influences the results only for southward IMF, while using the coupled model changes N both for northward and southward IMF. Simulations with a higher grid resolution at the subsolar magnetopause also yield the power law with a smaller N. Note also that the magnetopause position in the LFM-MIX model for southward IMF is not stable (because of reconnection), therefore the estimations of N may be less accurate.

3 Discussion and Conclusions

Most empirical magnetopause models assume a general relation between the solar wind dynamic pressure and the magnetopause standoff distance (1), where N remains constant for all solar wind conditions. We make a series of MHD runs to check this assumption. In the artificial runs, we change only one solar wind plasma parameter, either the density or velocity, getting the same step-like increases in the dynamic pressure in both cases. We make the simulations for northward and southward IMF and calculate the power law index N. We compare several versions of the SWMF and LFM-MIX models and obtain similar trends for all models as explained below.

In all cases, N is largest (≥ 7 in 5 of 6 cases) for the density increase and southward IMF. In most cases, N is smallest for the velocity increase both for the northward and southward IMF. A smaller N means larger variations of the R_{SUB} for the same changes in the dynamic pressure. We also compare the CPCP and the magnetic field in the subsolar point at geosynchronous orbit for these runs and obtain the greatest CPCP and weakest magnetic field for the run with high velocities and southward IMF. Summarizing these results, we conclude that the increase in the solar wind velocity for southward IMF enhances the magnetopause reconnection rate and dayside Region 1 currents and moves the magnetopause closer to the Earth than it appears in the case of density increase for the same IMF and dynamic pressure. Note that most empirical magnetopause models use the IMF B_z as an input parameter, but that they do not allow IMF B_z to influence the index N. We show here that N, in general, depends on the IMF orientation, and, moreover, it depends on which parameter, density or velocity, produces P_d variations. We suggest that a new generation of empirical magnetopause models would be more accurate using a new relation

$$R_{SUB} \sim \rho_{SW}^{-1/N} V_{SW}^{-2/M} \tag{2}$$

where $M \neq N$ and both M and N may depend on the sign of B_z.

Our results also show that increase in the ionospheric conductivity or the use of a model with the additional inner magnetosphere - ionosphere block result in decrease in N. Therefore we cannot derive a single N from the MHD simulations because the dis-

persion in N between the models is large, however all models predict the same changes between different runs related to the density and velocity increases, and B_z sign.

The simulations we present suggest that dayside magnetopause reconnection influences the magnetic field magnitude at geosynchronous orbit near subsolar point. We obtain different geosynchronous magnetic fields in northward and southward IMF runs with the same dynamic pressure. Moreover, the magnetic field magnitude is also different when comparing the runs in which both the dynamic pressure and B_z are kept the same and only the ratio between the solar wind ρ and V is different. Increasing velocity instead of density for a southward IMF, we increase the magnetopause reconnection rate and this results in an observable difference in the magnetic field at geosynchronous orbit with a smaller $|B|$ corresponding to a larger V_{SW}. Similar variations at geosynchronous orbit are observed in northward/southward turning events with a constant solar wind dynamic pressure (Samsonov et al., 2017).

Our results partly agree with the results in Němeček et al. (2016). We find that an increase in the ionospheric conductivity causes stronger variations of the magnetopause standoff distance, but, contrary to Němeček et al. (2016), an increase in the solar wind velocity may also enhance variations of the standoff distance. However, we cannot compare our results with Němeček et al. (2016) directly. Němeček et al. (2016) normalized observed R_{SUB} by the (Shue et al., 1997) model and obtained that the model underestimates R_{SUB} for high velocities. First, we note that it would agree with a numerical model for which $N > 6.6$ since $N = 6.6$ in (Shue et al., 1997). Second, variations of the solar wind velocity cannot be treated independently in the observations, they correlate with variations of the magnetic field (Owens & Cargill, 2002), and even (on a large time scale) with the ionospheric conductivity because higher velocities are usually observed at solar maximum. Therefore it is difficult to make a straightforward conclusion from these results.

In our work, we use only MHD simulations and make runs with the artificial solar wind conditions. However, we believe that MHD models reproduce reasonably well the magnetopause standoff distance for typical solar wind conditions (Samsonov et al., 2016). We anticipate that this work will help in the development of future empirical magnetopause models. One of the forthcoming missions which will study variations of the dayside magnetopause is the Solar Wind Magnetosphere Ionosphere Link Explorer (SMILE) (Raab et al., 2016). Using SMILE, we will be able to obtain a continuous time series of the magnetopause standoff distance for variable solar wind conditions and also validate prospective empirical models.

Acknowledgments

This work was carried out using the SWMF/BATSRUS tools developed at The University of Michigan Center for Space Environment Modeling and the LFM–MIX model available through the NASA Community Coordinated Modeling Center (http://ccmc.gsfc.nasa.gov). In particular, we used results of the runs *Andrey_Samsonov_072419_(1-4)*. AAS and GBR acknowledge support from the UK Space Agency under grant ST/R002258/1. YVB is supported by the STFC RAL Space IHR grant.

References

Aubry, M. P., Russell, C. T., & Kivelson, M. G. (1970). Inward motion of the magnetopause before a substorm. *Journal of Geophysical Research*, *75*(34), 7018-7031. doi: 10.1029/JA075i034p07018

Beard, D. B. (1960, November). The Interaction of the Terrestrial Magnetic Field with the Solar Corpuscular Radiation. *Journal of Geophysical Research*, *65*, 3559. doi: 10.1029/JZ065i011p03559

Borovsky, J. E., & Birn, J. (2014). The solar wind electric field does not control the dayside reconnection rate. *Journal of Geophysical Research: Space Physics*, *119*(2), 751-760. doi: 10.1002/2013JA019193

Borovsky, J. E., Hesse, M., Birn, J., & Kuznetsova, M. (2008). What determines the reconnection rate at the dayside magnetosphere? *Journal of Geophysical Research: Space Physics*, *113*(A7). doi: 10.1029/2007JA012645

Cassak, P. A., & Shay, M. A. (2007). Scaling of asymmetric magnetic reconnection: General theory and collisional simulations. *Physics of Plasmas*, *14*(10), 102114. doi: 10.1063/1.2795630

Chapman, S., & Ferraro, V. C. A. (1931). A new theory of magnetic storms. *Terrestrial Magnetism and Atmospheric Electricity*, *36*(2), 77-97. doi: 10.1029/TE036i002p00077

Dušík, v., Granko, G., Šafránková, J., Němeček, Z., & Jelínek, K. (2010). Imf cone angle control of the magnetopause location: Statistical study. *Geophysical Research Letters*, *37*(19). doi: 10.1029/2010GL044965

Fairfield, D. H. (1971). Average and unusual locations of the earth's magnetopause and bow shock. *Journal of Geophysical Research (1896-1977)*, *76*(28), 6700-6716. doi: 10.1029/JA076i028p06700

Fok, M.-C., Buzulukova, N. Y., Chen, S.-H., Glocer, A., Nagai, T., Valek, P., & Perez, J. D. (2014). The comprehensive inner magnetosphere-ionosphere model. *Journal of Geophysical Research: Space Physics*, *119*(9), 7522-7540. doi: 10.1002/2014JA020239

Freeman, M. P., Freeman, N. C., & Farrugia, C. J. (1995). A linear perturbation analysis of magnetopause motion in the newton-busemann limit. *Annales Geophysicae*, *13*(9), 907–918. doi: 10.1007/s00585-995-0907-0

Grygorov, K., Šafránková, J., Němeček, Z., Pi, G., Přech, L., & Urbář, J. (2017, November). Shape of the equatorial magnetopause affected by the radial interplanetary magnetic field. *Planetary and Space Science*, *148*, 28-34. doi: 10.1016/j.pss.2017.09.011

Hill, T. W., Dessler, A. J., & Wolf, R. A. (1976). Mercury and mars: The role of ionospheric conductivity in the acceleration of magnetospheric particles. *Geophysical Research Letters*, *3*(8), 429-432. doi: 10.1029/GL003i008p00429

Hill, T. W., & Rassbach, M. E. (1975). Interplanetary magnetic field direction and the configuration of the day side magnetosphere. *Journal of Geophysical Research*, *80*(1), 1-6. doi: 10.1029/JA080i001p00001

Lin, R. L., Zhang, X. X., Liu, S. Q., Wang, Y. L., & Gong, J. C. (2010). A three-dimensional asymmetric magnetopause model. *Journal of Geophysical Research (Space Physics)*, *115*, A04207. doi: 10.1029/2009JA014235

Liu, Z.-Q., Lu, J. Y., Wang, C., Kabin, K., Zhao, J. S., Wang, M., ... Zhao, M. X. (2015, jul). A three-dimensional high mach number asymmetric magnetopause model from global mhd simulation. *Journal of Geophysical Research (Space Physics)*, *120*, 5645-5666. doi: 10.1002/2014JA020961

Lu, J. Y., Liu, Z.-Q., Kabin, K., Zhao, M. X., Liu, D. D., Zhou, Q., & Xiao, Y. (2011). Three dimensional shape of the magnetopause: Global mhd results. *Journal of Geophysical Research: Space Physics*, *116*(A9). doi: 10.1029/2010JA016418

Lyon, J. G., Fedder, J. A., & Mobarry, C. M. (2004, October). The Lyon-Fedder-Mobarry (LFM) global MHD magnetospheric simulation code. *Journal of Atmospheric and Solar-Terrestrial Physics*, *66*, 1333-1350. doi: 10.1016/j.jastp.2004.03.020

Merka, J., Szabo, A., Šafránková, J., & Němeček, Z. (2003). Earth's bow shock and magnetopause in the case of a field-aligned upstream flow: Observation and model comparison. *Journal of Geophysical Research: Space Physics*, *108*(A7). doi: 10.1029/2002JA009697

Merkin, V. G., & Lyon, J. G. (2010). Effects of the low-latitude ionospheric bound-

ary condition on the global magnetosphere. *Journal of Geophysical Research: Space Physics*, *115*(A10). doi: 10.1029/2010JA015461

Němeček, Z., Šafránková, J., Koval, A., Merka, J., & Přech, L. (2011, January). MHD analysis of propagation of an interplanetary shock across magnetospheric boundaries. *Journal of Atmospheric and Solar-Terrestrial Physics*, *73*, 20-29. doi: 10.1016/j.jastp.2010.05.017

Němeček, Z., Šafránková, J., Lopez, R. E., Dušík, Š., Nouzák, L., Přech, L., ... Shue, J.-H. (2016, July). Solar cycle variations of magnetopause locations. *Advances in Space Research*, *58*, 240-248. doi: 10.1016/j.asr.2015.10.012

Owens, M. J., & Cargill, P. J. (2002). Correlation of magnetic field intensities and solar wind speeds of events observed by ace. *Journal of Geophysical Research: Space Physics*, *107*(A5), SSH 1-1-SSH 1-7. doi: 10.1029/2001JA000238

Petrinec, S. M., & Russell, C. T. (1996). Near-Earth magnetotail shape and size as determined from the magnetopause flaring angle. *J. Geophys. Res.*, *101*, 137-152. doi: 10.1029/95JA02834

Raab, W., Branduardi-Raymont, G., Dai, L., Wang, C., Donovan, E., Enno, G., ... Zheng, J. (2016). Smile: a joint esa/cas mission to investigate the interaction between the solar wind and earth's magnetosphere. In *Space telescopes and instrumentation 2016: Ultraviolet to gamma ray* (Vol. 9905, p. 990502).

Roelof, E. C., & Sibeck, D. G. (1993). Magnetopause shape as a bivariate function of interplanetary magnetic field B_z and solar wind dynamic pressure. *J. Geophys. Res.*, *98*, 21. doi: 10.1029/93JA02362

Samsonov, A. A., Gordeev, E., Tsyganenko, N. A., Šafránková, J., Němeček, Z., Šimunek, J., ... Raeder, J. (2016, July). Do we know the actual magnetopause position for typical solar wind conditions? *Journal of Geophysical Research (Space Physics)*, *121*, 6493-6508. doi: 10.1002/2016JA022471

Samsonov, A. A., & Sibeck, D. G. (2013, June). Large-scale flow vortices following a magnetospheric sudden impulse. *Journal of Geophysical Research (Space Physics)*, *118*, 3055-3064. doi: 10.1002/jgra.50329

Samsonov, A. A., Sibeck, D. G., & Imber, J. (2007, December). MHD simulation for the interaction of an interplanetary shock with the Earth's magnetosphere. *Journal of Geophysical Research (Space Physics)*, *112*, A12220. doi: 10.1029/2007JA012627

Samsonov, A. A., Sibeck, D. G., Šafránková, J., Němeček, Z., & Shue, J.-H. (2017). A method to predict magnetopause expansion in radial imf events by mhd simulations. *Journal of Geophysical Research: Space Physics*, *122*(3), 3110-3126. doi: 10.1002/2016JA023301

Samsonov, A. A., Sibeck, D. G., Zolotova, N. V., Biernat, H. K., Chen, S.-H., Rastaetter, L., ... Baumjohann, W. (2011). Propagation of a sudden impulse through the magnetosphere initiating magnetospheric pc5 pulsations. *Journal of Geophysical Research: Space Physics*, *116*(A10). doi: 10.1029/2011JA016706

Shue, J.-H., Chao, J. K., Fu, H. C., Russell, C. T., Song, P., Khurana, K. K., & Singer, H. J. (1997). A new functional form to study the solar wind control of the magnetopause size and shape. *Journal of Geophysical Research: Space Physics*, *102*(A5), 9497-9511. doi: 10.1029/97JA00196

Shue, J.-H., Song, P., Russell, C. T., Steinberg, J. T., Chao, J. K., Zastenker, G., ... Kawano, H. (1998). Magnetopause location under extreme solar wind conditions. *J. Geophys. Res.*, *103*, 17691-17700. doi: 10.1029/98JA01103

Sibeck, D. G. (1994, May). Signatures of flux erosion from the dayside magnetosphere. *Journal of Geophysical Research*, *99*, 8513-8529. doi: 10.1029/93JA03298

Sibeck, D. G., Lopez, R. E., & Roelof, E. C. (1991). Solar wind control of the magnetopause shape, location, and motion. *Journal of Geophysical Research: Space Physics*, *96*(A4), 5489-5495. doi: 10.1029/90JA02464

Siscoe, G. L., Erickson, G. M., Sonnerup, B. U. ., Maynard, N. C., Schoendorf, J. A., Siebert, K. D., ... Wilson, G. R. (2002). Hill model of transpolar potential saturation: Comparisons with mhd simulations. *Journal of Geophysical Research*, *107*(A6), SMP 8-1-SMP 8-8. doi: 10.1029/2001JA000109

Suvorova, A. V., & Dmitriev, A. V. (2015). Magnetopause inflation under radial imf: Comparison of models. *Earth and Space Science*, *2*(4), 107-114. doi: 10.1002/2014EA000084

Suvorova, A. V., Shue, J.-H., Dmitriev, A. V., Sibeck, D. G., McFadden, J. P., Hasegawa, H., ... Němeček, Z. (2010). Magnetopause expansions for quasi-radial interplanetary magnetic field: Themis and geotail observations. *J. Geophys. Res.*, *115*(A10). doi: 10.1029/2010JA015404

Tóth, G., Sokolov, I. V., Gombosi, T. I., Chesney, D. R., Clauer, C. R., de Zeeuw, D. L., ... Kóta, J. (2005, December). Space Weather Modeling Framework: A new tool for the space science community. *Journal of Geophysical Research (Space Physics)*, *110*, A12226. doi: 10.1029/2005JA011126

Tóth, G., van der Holst, B., Sokolov, I. V., De Zeeuw, D. L., Gombosi, T. I., Fang, F., ... Opher, M. (2012, February). Adaptive numerical algorithms in space weather modeling. *Journal of Computational Physics*, *231*, 870-903. doi: 10.1016/j.jcp.2011.02.006

Tsyganenko, N. A., & Sibeck, D. G. (1994). Concerning flux erosion from the dayside magnetosphere. *Journal of Geophysical Research: Space Physics*, *99*(A7), 13425-13436. doi: 10.1029/94JA00719

Table 1. Index N in expression $R_{SUB} \sim P_d^{-1/N}$ obtained in MHD simulations. Runs: 1 – the non-coupled SWMF (v20140611), 2 – the same non-coupled SWMF with ionospheric conductivity of 10 S instead of 5 S, 3 – the same model with a very large ionospheric conductivity 100 S, 4 – the same model with a dipole tilt 30° in xz plane, 5 – the SWMF SIMI (inner magnetosphere-ionosphere) v20180525, 6 – the LFM-MIX. The words "Density" and "Velocity" indicate that only density and velocity have been increased, "Northward" and "Southward" mean the IMF orientation.

Model	1	2	3	4	5	6
Density/Northward	6.53	6.51	6.31	6.27	5.95	6.40
Velocity/Northward	6.23	6.19	6.24	6.48	5.92	6.30
Density/Southward	7.80	7.82	7.00	7.51	6.32	7.98
Velocity/Southward	6.69	6.16	6.21	6.64	5.83	6.38

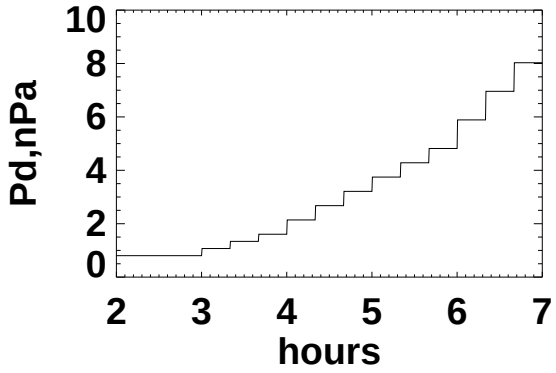

Figure 1. Input solar wind conditions: dynamic pressure.

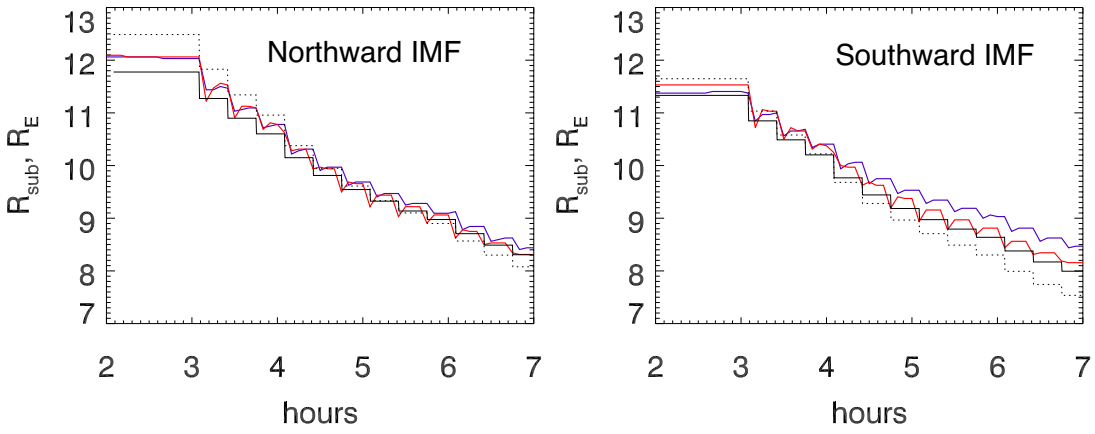

Figure 2. Left panel (runs 1-2), right panel (runs 3-4). Blue and red lines correspond to density (runs 1,3) and velocity increases (runs 2,4) in the noncoupled SWMF model. Results of the empirical (Shue et al., 1998) (black solid) and (Lin et al., 2010) (black dotted) models are shown for comparison.

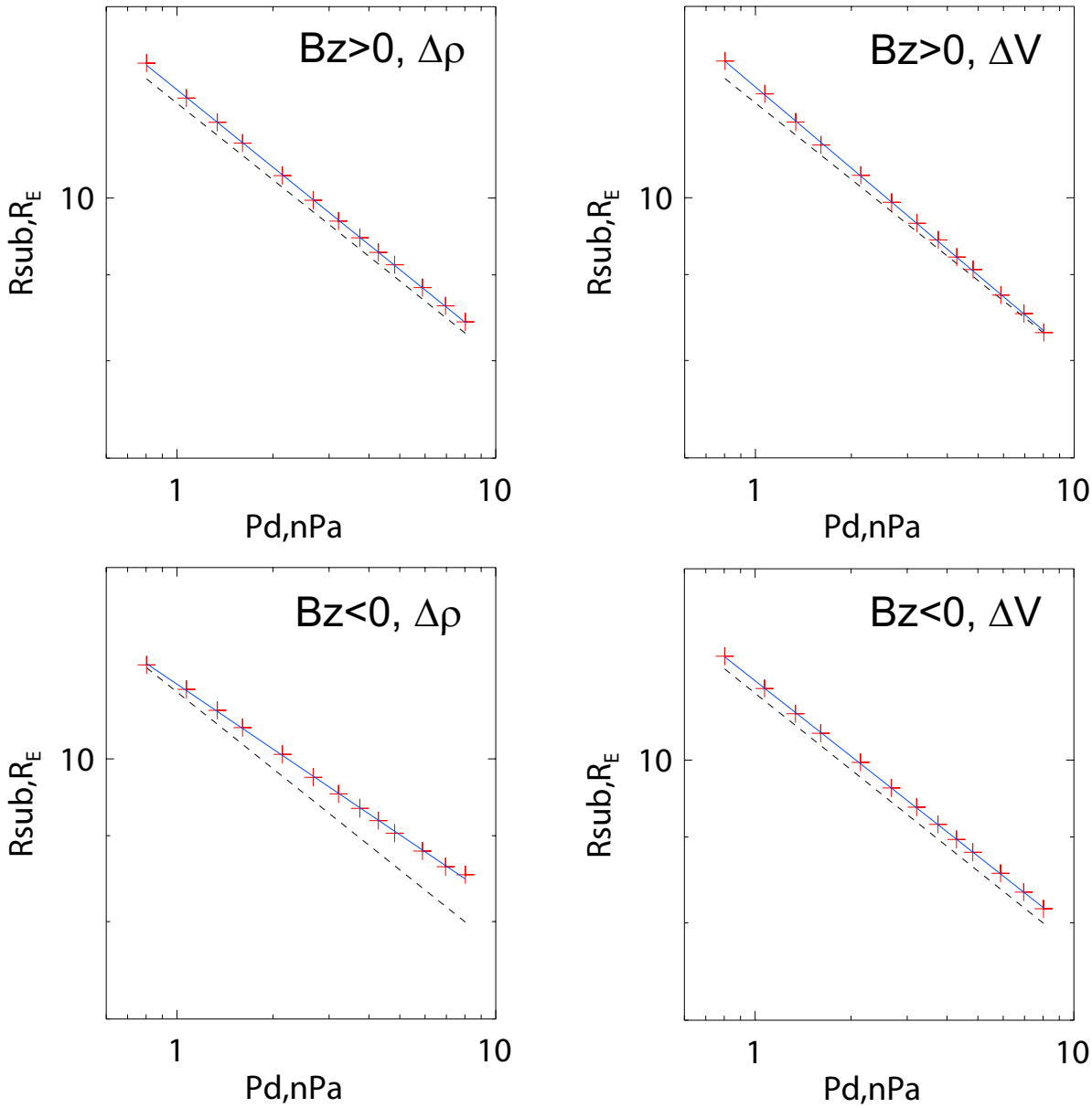

Figure 3. R_{SUB} dependence on P_d in runs 1-4 of the noncoupled SWMF model. Red crosses correspond to MHD results, and blue lines show linear interpolation for these points. Black dashed lines display the results of the empirical (Shue et al., 1998) model.

Figure 1.

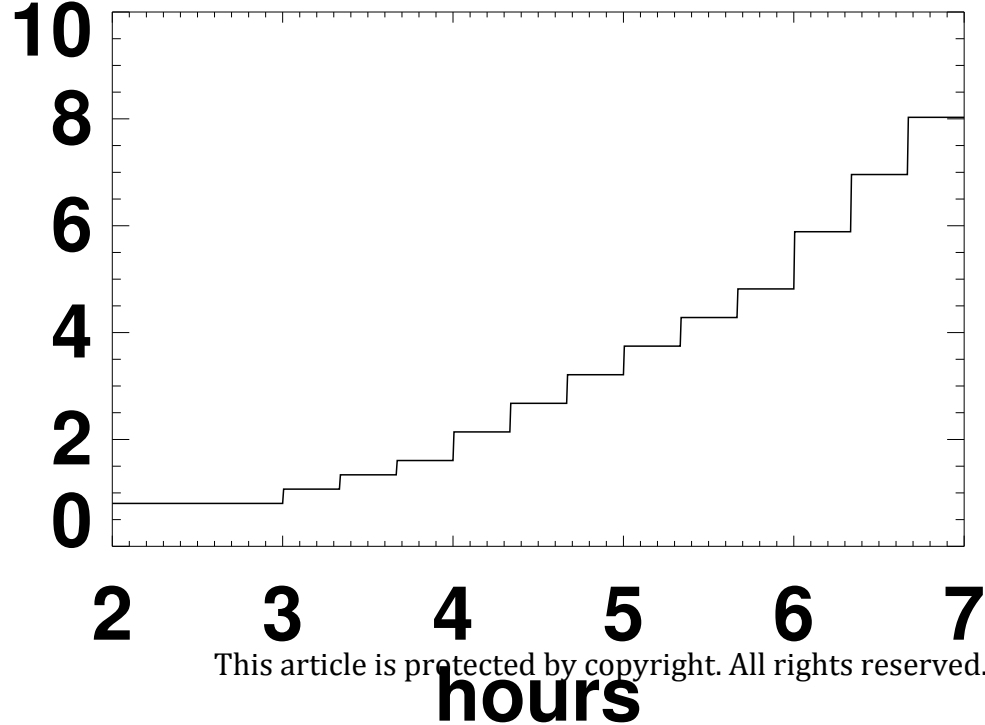

Figure 2.

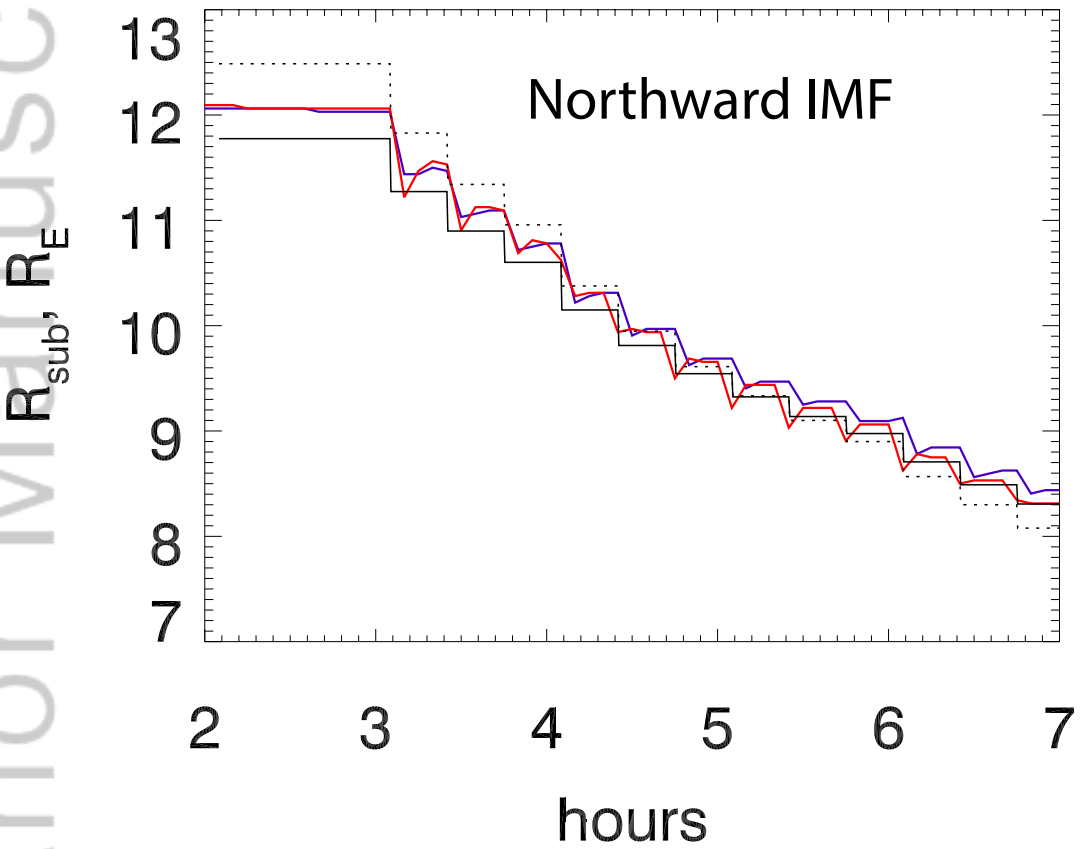

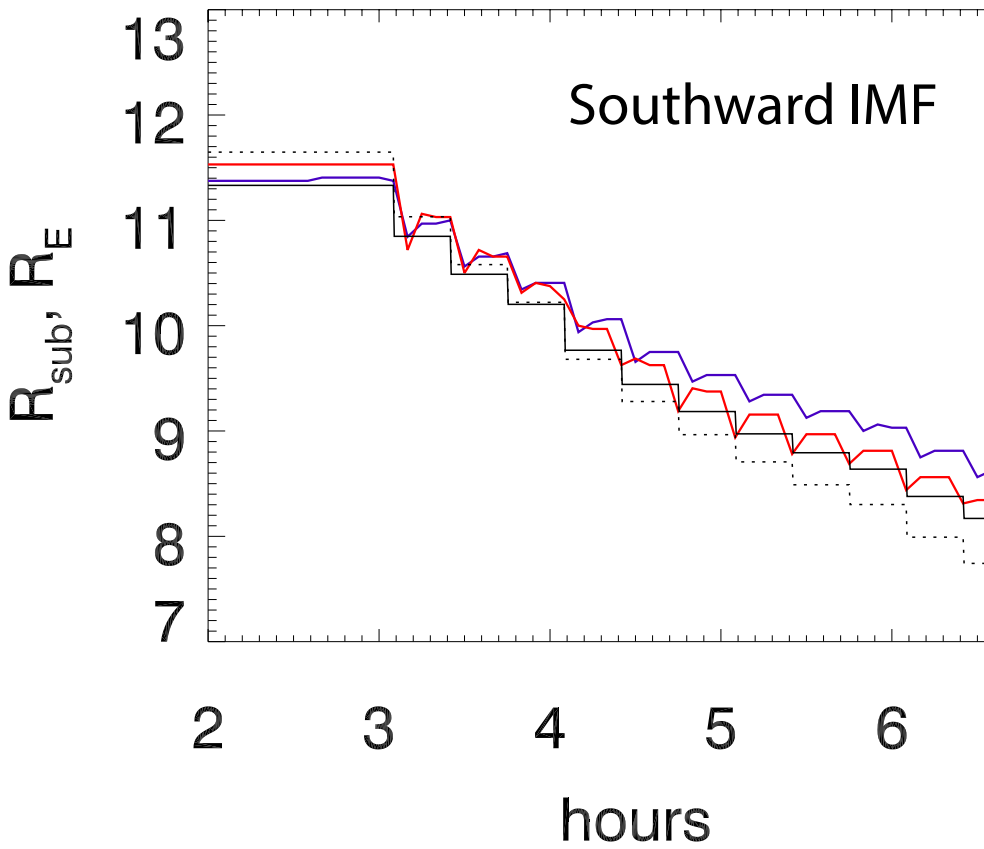

Figure 3.

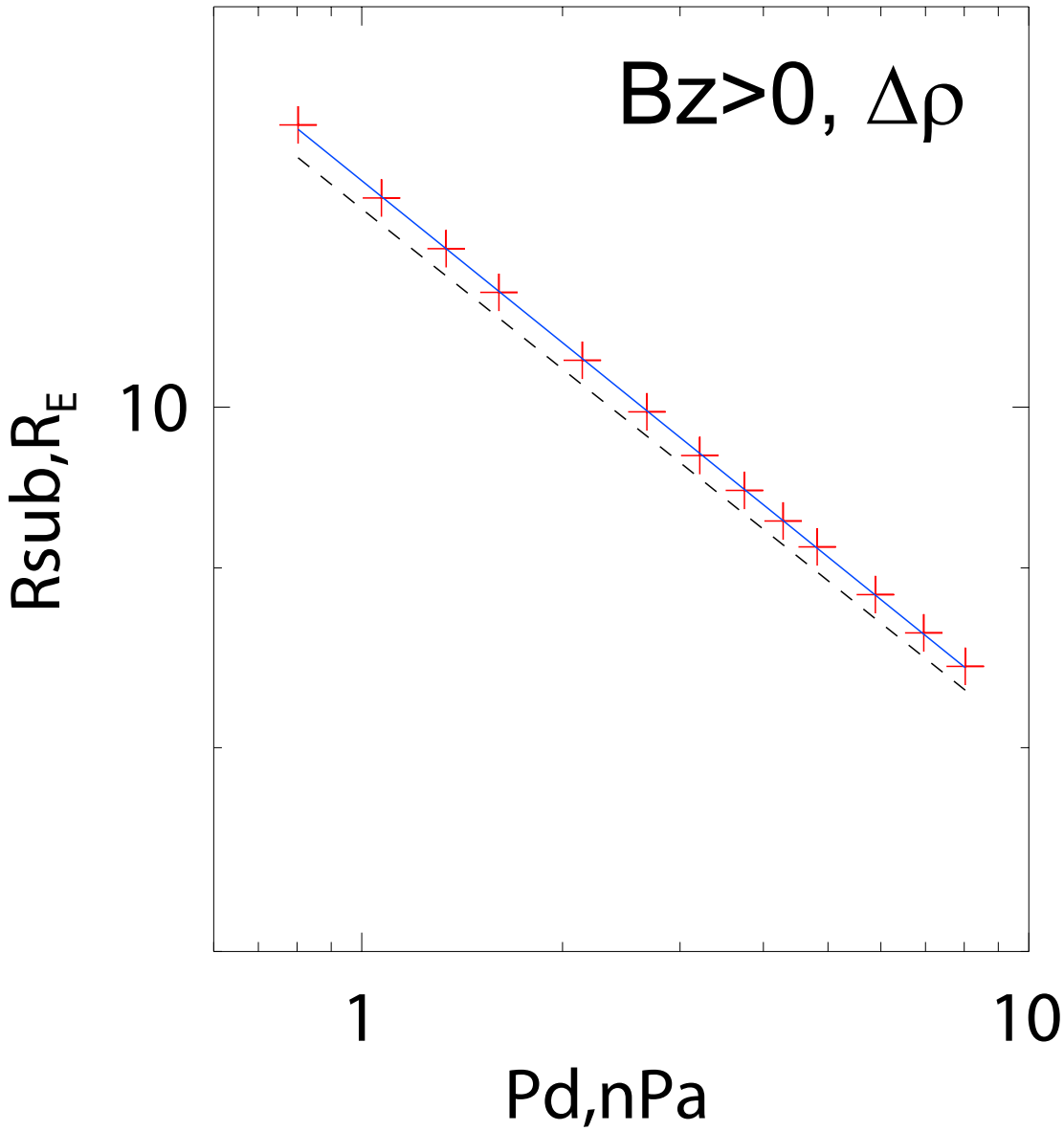

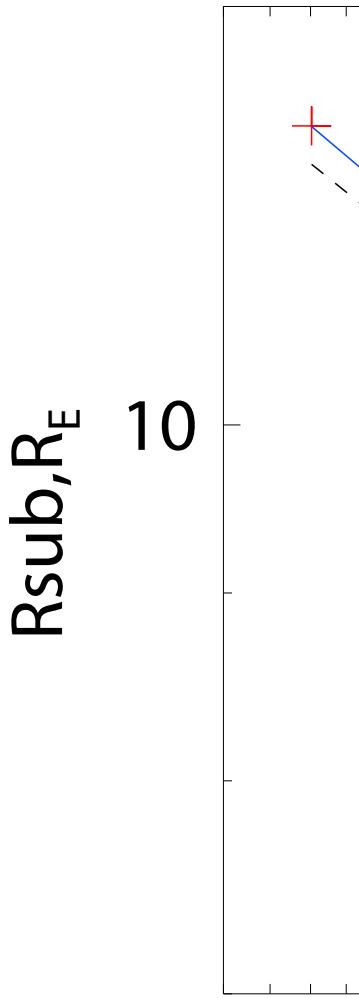

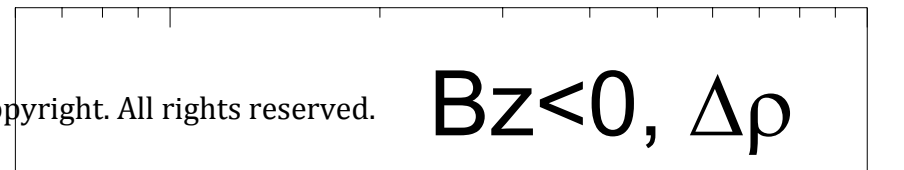

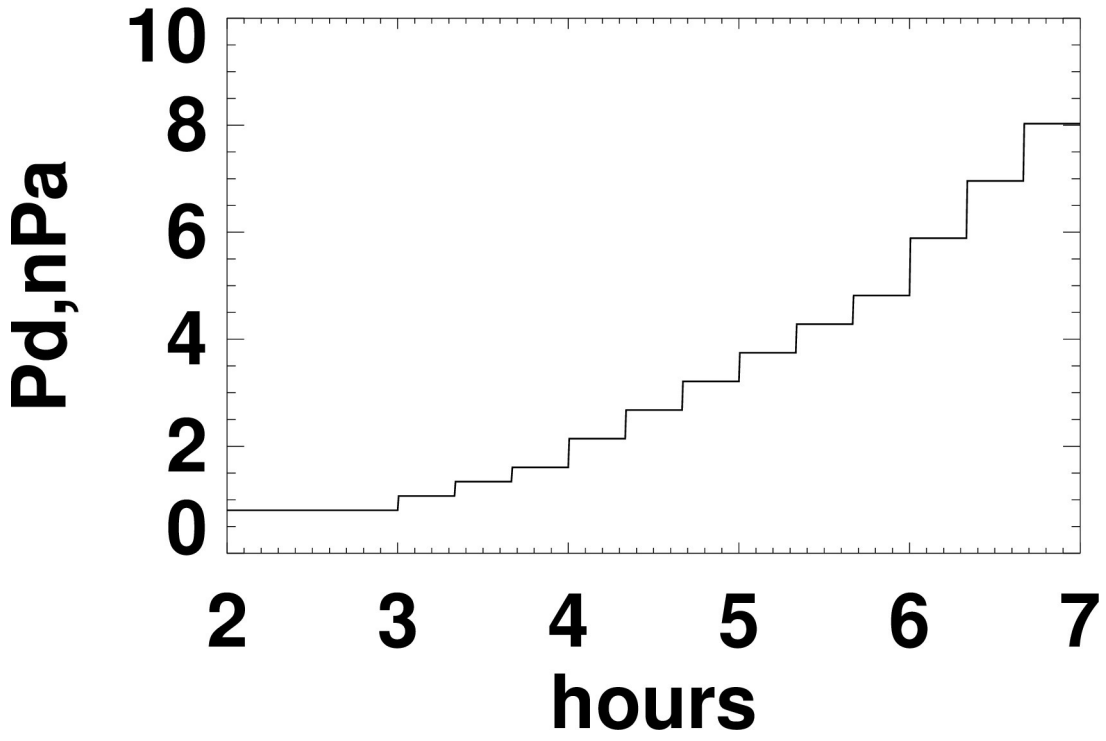

2019gl086474-f01-z-.eps

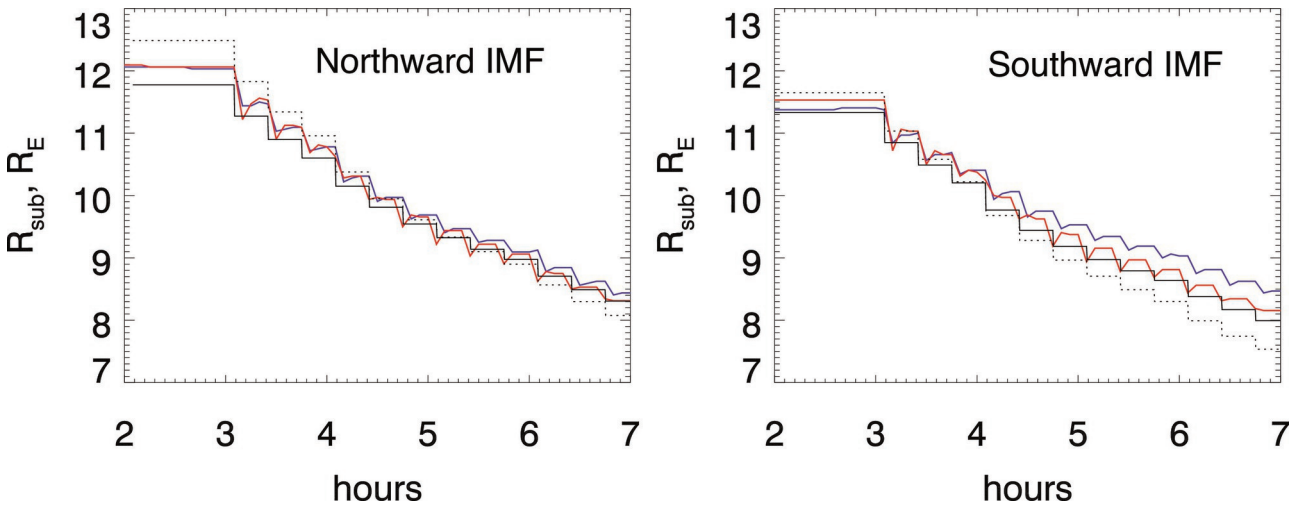

2019gl086474-f02-z-.eps

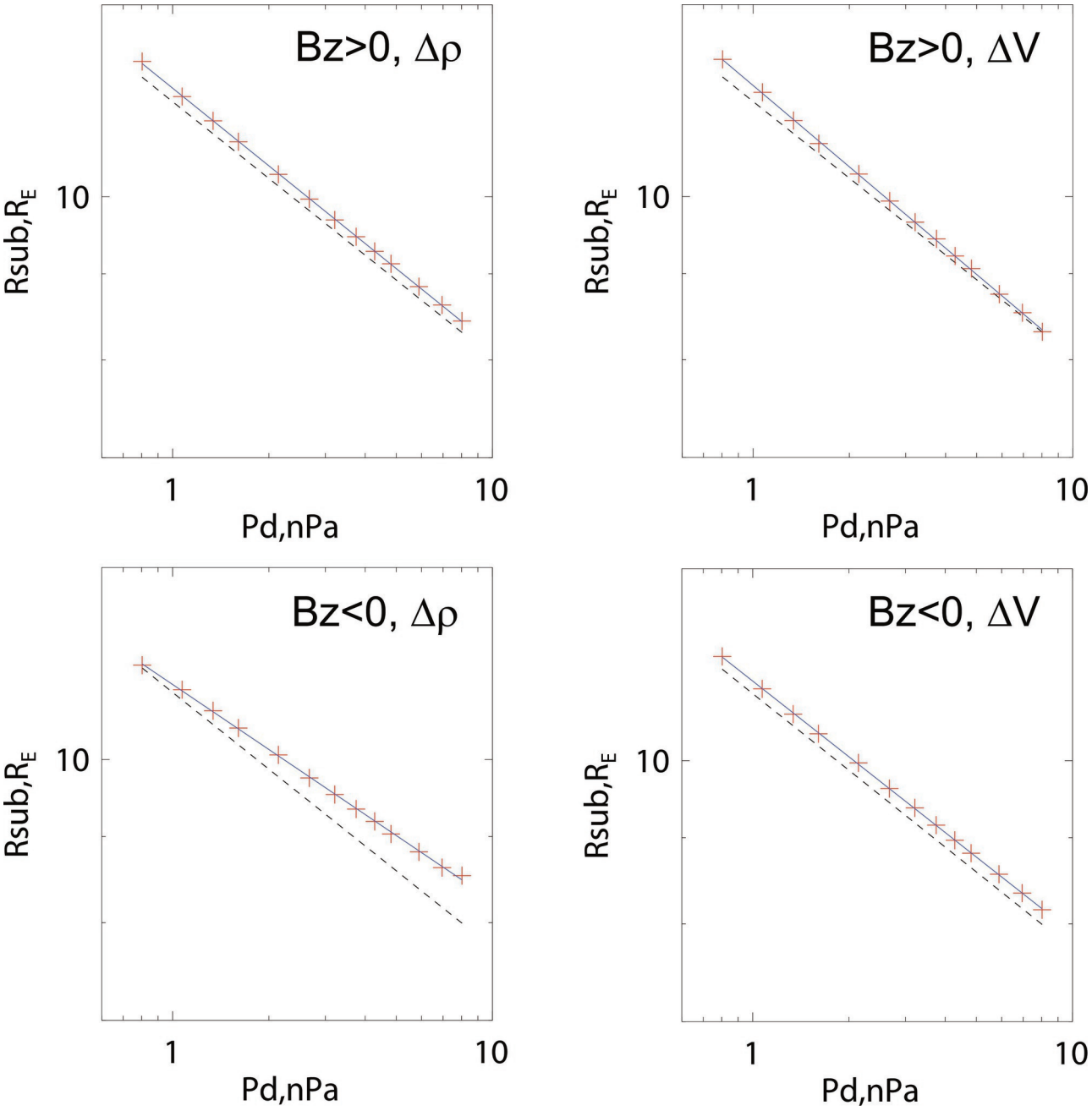

2019gl086474-f03-z-.eps